2 kb (327) were subsequently removed, leaving 1,425 scaffolds with a combined size of 25,393,225 bp. The remaining scaffolds were analysed to remove redundancy that may have resulted as a consequence of allelic differences or aneuploidy. We removed all scaffolds smaller than 5 kb that shared 98% or more nucleotide sequence identity over greater than 95% of their lengths. Removal of these scaffolds left 888 scaffolds remaining, with a total length of 23,751,783 bp. All scaffolds removed during the clean-up process as well as any singleton reads, although not used in the annotation process, were used in determining the presence or absence of genes in the *E. histolytica* genome. Unfortunately, there is no map to order the scaffolds generated by the assembly; however, the sequence generated by this project should assist in making maps for this genome in the future, and although the large-scale structure of the genome has been lost, the vast majority of the genes that have been predicted are full length with intact 3′ and 5′ untranslated regions.

Annotation

The Combiner algorithm was used for gene structure identification[22] using two genefinder programs, phat[23] and GlimmerHMM[24], trained using a set of published *E. histolytica* gene sequences, alignments of protein homologues to the genomic sequence and alignment of a set of *E. histolytica* complementary DNA sequences (provided by N. Guillén) to the genomic sequence. The Combiner gene predictions were then manually curated. Functional annotations for the predicted proteins were automatically generated using a combination of numerous sources of evidence including searches against a non-redundant protein database and identification of functional domains by searches against the Pfam database[25]. tRNAs were detected using the tRNAscan-SE[26] program with default parameters.

Identification of sequence homologues in other species

Sequence homologues from other species were identified by searching the predicted proteins from the *E. histolytica* genome against the publicly available nr database of GenBank using BlastP (http://www.ncbi.nlm.nih.gov/BLAST/) and filtering search results with an *e*-value of 10^{-5} or less, which was chosen because of the relatively large divergence between *E. histolytica* and other organisms for which the genomes have been sequenced and for which protein data are available.

Phylogenetic analysis

We modified a published suite of scripts and modules called PyPhy[27] to make an automated genome-wide primary screen for LGT. PyPhy was used to make bootstrap (100 replicates) consensus *p*-distance trees from edited alignments of 5,740 *E. histolytica* proteins; that is, those for which there were sufficient homologues (>4) in SwissProt and TrEMBL to make trees. The trees were analysed to identify cases where the nearest neighbour to the *E. histolytica* protein was a prokaryotic sequence. As an additional screen for LGT we identified all proteins for which a prokaryote was the top Blast hit. After manual inspection of the alignments, Blast outputs, tree support values and sequence identities, 279 cases of potential LGT were retained for more detailed phylogenetic analyses. Each candidate LGT was analysed by MrBayes[28] using the WAG matrix, a gamma correction for site rate variation and a proportion (pinvar) of invariant sites. The analyses were run for 600,000 generations and sampled every 100 generations, with the first 2,000 samples discarded as burn-in. A consensus tree was made from the remaining samples. Because posterior probabilities—the support values used by bayesian analysis to indicate confidence in groups—have been criticized[29], we also used bootstrapping to provide an additional indication of support for relationships. Each data set was bootstrapped (100 replicates) and used to make distance matrices under the same evolutionary model as in the bayesian analysis, using custom (P4) software (available on request). Trees were made from the distance matrices using FastME[30] and a bootstrap consensus tree made using P4. On the basis of these analyses we identified 96 genes in which the tree topology is consistent with prokaryote to eukaryote LGT. Blast summary statistics, trees and support values for these 96 candidate LGT are provided as Supplementary Information.

Received 26 October; accepted 2 December 2004; doi:10.1038/nature03291.

1. Stanley, S. L. Jr Amoebiasis. *Lancet* **361,** 1025–1034 (2003).
2. Pataraportikul, J. & Langsley, G. Chromosome size polymorphism in *Plasmodium falciparum* can involve deletions of the subtelomeric pPFrep20 sequence. *Nucleic Acids Res.* **16,** 4331–4340 (1988).
3. Melville, S. E., Gerrard, C. S. & Blackwell, J. M. Multiple causes of size variation in the diploid megabase chromosomes of African trypanosomes. *Chromosome Res.* **7,** 191–203 (1999).
4. Leon-Avila, G. & Tovar, J. Mitosomes of *Entamoeba histolytica* are abundant mitochondrion-related remnant organelles that lack a detectable organellar genome. *Microbiology* **150,** 1245–1250 (2004).
5. Fahey, R. C., Newton, G. L., Arrick, B., Overdank-Bogart, T. & Aley, S. B. *Entamoeba histolytica*: a eukaryote without glutathione metabolism. *Science* **224,** 70–72 (1984).
6. Abrahamsen, M. S. *et al.* Complete genome sequence of the apicomplexan, *Cryptosporidium parvum*. *Science* **304,** 441–445 (2004).
7. Baum, K. F., Berens, R. L., Marr, J. J., Harrington, J. A. & Spector, T. Purine deoxynucleoside salvage in *Giardia lamblia*. *J. Biol. Chem.* **264,** 21087–21090 (1989).
8. Jordan, I. K., Henze, K., Fedorova, N. D., Koonin, E. V. & Galperin, M. Y. Phylogenomic analysis of the *Giardia intestinalis* transcarboxylase reveals multiple instances of domain fusion and fission in the evolution of biotin-dependent enzymes. *J. Mol. Microbiol. Biotechnol.* **5,** 172–189 (2003).
9. James, D. W. Jr *et al.* Directed tagging of the *Arabidopsis* fatty acid elongation1 (FAE1) gene with the maize transposon activator. *Plant Cell* **7,** 309–319 (1995).
10. Azachi, M. *et al.* Salt induction of fatty acid elongase and membrane lipid modifications in the extreme halotolerant alga *Dunaliella salina*. *Plant Physiol.* **129,** 1320–1329 (2002).
11. Lawrence, J. G. & Hendrickson, H. Lateral gene transfer: when will adolescence end? *Mol. Microbiol.* **50,** 739–749 (2003).
12. Huston, C. D. Parasite and host contributions to the pathogenesis of amebic colitis. *Trends Parasitol.* **20,** 23–26 (2004).
13. Welter, B. H. & Temesvari, L. A. A unique Rab GTPase, EhRabA, of *Entamoeba histolytica*, localizes to the leading edge of motile cells. *Mol. Biochem. Parasitol.* **135,** 185–195 (2004).
14. Mazzuco, A., Benchimol, M. & De Souza, W. Endoplasmic reticulum and Golgi-like elements in *Entamoeba*. *Micron* **28,** 241–247 (1997).
15. Duhon, D. & Cardelli, J. The regulation of phagosome maturation in *Dictyostelium*. *J. Muscle Res. Cell Motil.* **23,** 803–808 (2002).
16. Voigt, H. & Guillen, N. New insights into the role of the cytoskeleton in phagocytosis of *Entamoeba histolytica*. *Cell. Microbiol.* **1,** 195–203 (1999).
17. Hunter, T. Protein kinase classification. *Methods Enzymol.* **200,** 3–37 (1991).
18. Coppi, A., Merali, S. & Eichinger, D. The enteric parasite *Entamoeba* uses an autocrine catecholamine system during differentiation into the infectious cyst stage. *J. Biol. Chem.* **277,** 8083–8090 (2002).
19. Gomes, C. M. *et al.* A novel type of nitric-oxide reductase. *Escherichia coli* flavorubredoxin. *J. Biol. Chem.* **277,** 25273–25276 (2002).
20. Sztukowska, M., Bugno, M., Potempa, J., Travis, J. & Kurtz, D. M. Jr Role of rubrerythrin in the oxidative stress response of *Porphyromonas gingivalis*. *Mol. Microbiol.* **44,** 479–488 (2002).
21. Mullikin, J. C. & Ning, Z. The phusion assembler. *Genome Res.* **13,** 81–90 (2003).
22. Allen, J. E., Pertea, M. & Salzberg, S. L. Computational gene prediction using multiple sources of evidence. *Genome Res.* **14,** 142–148 (2004).
23. Cawley, S. E., Wirth, A. I. & Speed, T. P. Phat–a gene finding program for *Plasmodium falciparum*. *Mol. Biochem. Parasitol.* **118,** 167–174 (2001).
24. Majoros, W. H., Pertea, M. & Salzberg, S. L. TigrScan and GlimmerHMM: two open-source ab initio eukaryotic gene-finders. *Bioinformatics* **20,** 2878–2879 (2004).
25. Bateman, A. *et al.* The Pfam protein families database. *Nucleic Acids Res.* **32,** D138–D141 (2004).
26. Lowe, T. M. & Eddy, S. R. tRNAscan-SE: a program for improved detection of transfer RNA genes in genomic sequence. *Nucleic Acids Res.* **25,** 955–964 (1997).
27. Sicheritz-Ponten, T. & Andersson, S. G. A phylogenomic approach to microbial evolution. *Nucleic Acids Res.* **29,** 545–552 (2001).
28. Huelsenbeck, J. P. & Ronquist, F. MRBAYES: Bayesian inference of phylogenetic trees. *Bioinformatics* **17,** 754–755 (2001).
29. Cummings, M. P. *et al.* Comparing bootstrap and posterior probability values in the four-taxon case. *Syst. Biol.* **52,** 477–487 (2003).
30. Desper, R. & Gascuel, O. Theoretical foundation of the balanced minimum evolution method of phylogenetic inference and its relationship to weighted least-squares tree fitting. *Mol. Biol. Evol.* **21,** 587–598 (2004).

Supplementary Information accompanies the paper on **www.nature.com/nature**.

Acknowledgements This work was supported by grants from the National Institute of Allergy and Infectious Disease and the Wellcome Trust.

Competing interests statement The authors declare that they have no competing financial interests.

Correspondence and requests for materials should be addressed to B.L. (bjloftus@tigr.org). Scaffold sequences have been deposited in GenBank under the project accession number AAFB00000000. Sequences and annotation are available at http://www.tigr.org/tdb/e2k1/eha1/.

Excitatory cortical neurons form fine-scale functional networks

Yumiko Yoshimura*, Jami L. M. Dantzker* & Edward M. Callaway

Systems Neurobiology Laboratories, The Salk Institute for Biological Studies, 10010 North Torrey Pines Road, La Jolla, California 92037, USA

* Present addresses: Department of Visual Neuroscience, Research Institute of Environmental Medicine, Nagoya University, Furo-cho, Chikusa-ku, Nagoya 464-8601, Japan (Y.Y.); Department of Neurology and Neurological Sciences, Stanford University, 300 Pasteur Drive, Room M016, Stanford, California 94305-5122, USA (J.L.M.D.)

The specificity of cortical neuron connections creates columns of functionally similar neurons spanning from the pia to the white matter[1–6]. Here we investigate whether there is an additional, finer level of specificity that creates subnetworks of excitatory neurons within functional columns. We tested for fine-scale specificity of connections to cortical layer 2/3 pyramidal neurons in rat visual cortex by using cross-correlation analyses of synaptic currents evoked by photostimulation. Recording simultaneously from adjacent layer 2/3 pyramidal cells, we find that when they are connected to each other (20% of all recorded pairs) they share common input from layer 4 and within layer 2/3. When adjacent layer 2/3 neurons are not connected to each other, they share very little (if any) common excitatory input from layers 4 and 2/3. In contrast, all layer 2/3 neurons share common excitatory input

from layer 5 and inhibitory input from layers 2/3 and 4, regardless of whether they are connected to each other. Thus, excitatory connections from layer 4 to layer 2/3 and within layer 2/3 form fine-scale assemblies of selectively interconnected neurons; inhibitory connections and excitatory connections from layer 5 link neurons across these fine-scale subnetworks. Relatively independent subnetworks of excitatory neurons are therefore embedded within the larger-scale functional architecture; this allows neighbouring neurons to convey information more independently than suggested by previous descriptions of cortical circuitry.

The cerebral cortex consists of a complex network of neuronal connections, the organization of which is believed to contribute critically to perception and behaviour. Over the last several decades, the idea of the 'functional column' has provided a dominant influence on studies of the organization and function of cortical circuits[1]. The specificities of connections that both create and maintain functional architecture are well established[1–7] and provide a substrate for interactions between neurons with similar functional attributes. However, each excitatory neuron connects to only a minority of others in the same column[8,9]. This sparse connectivity is consistent with two different scenarios, each of which has implications for the way that cortical circuits process information. In the first scenario, connections would be dependent on the spatial overlap of dendrites and axons, but would otherwise be determined probabilistically, independent of other connections in

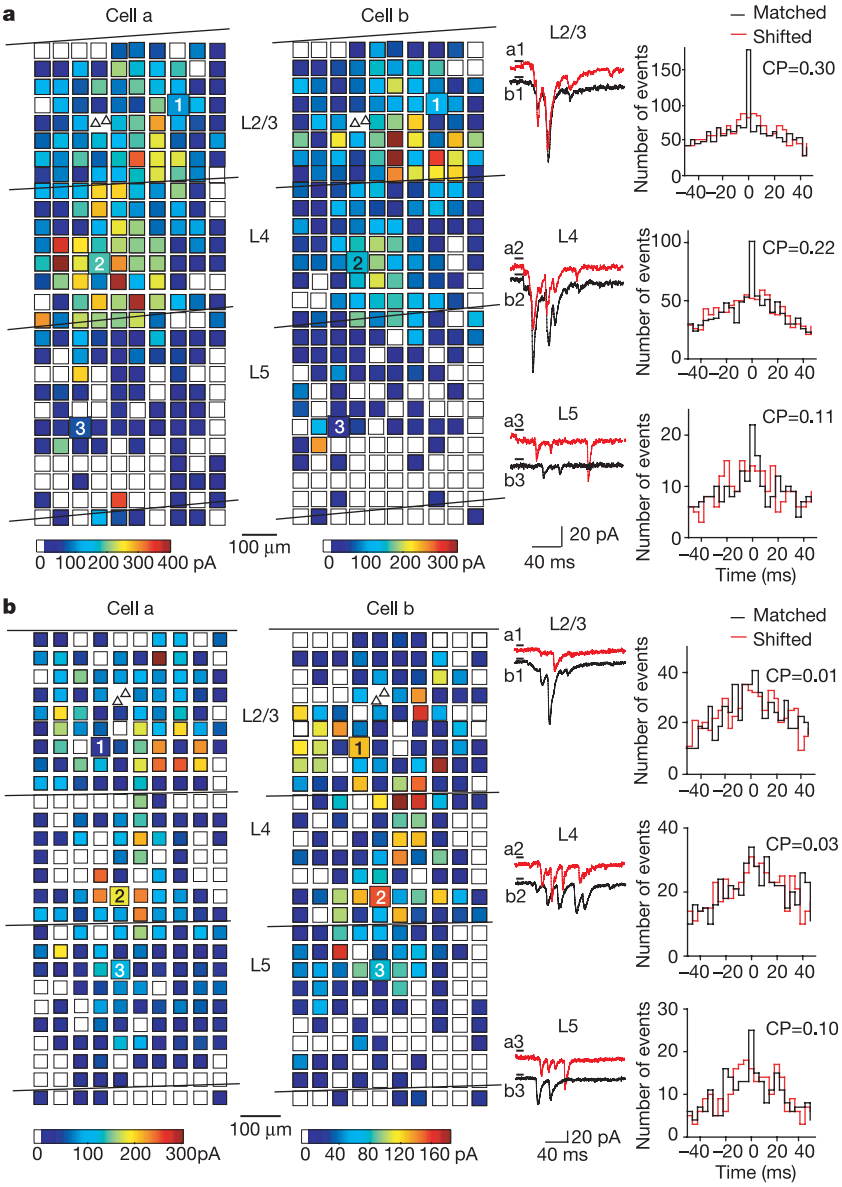

Figure 1 Cross-correlation analyses of photostimulation-evoked excitatory postsynaptic currents (EPSCs) simultaneously recorded in adjacent pairs of layer 2/3 pyramidal neurons. **a**, **b**, Results are shown for a pair of pyramidal neurons that was synaptically connected (**a**) and for a pair that was not connected (**b**). For each of the two cells, reconstructions of the locations of photostimulation sites (coloured squares) relative to the locations of laminar borders and cell bodies of recorded pyramidal neurons (triangles) are shown. The colour of each square indicates the sum of amplitudes of EPSCs that were observed in response to photostimulation at that site. To the right of these plots, example voltage clamp recordings are shown for stimulation sites indicated by the large numbered squares. Simultaneous recordings from representative sites in each cortical layer are shown for 'cell a' (red) and 'cell b' (black). The short horizontal lines above each trace indicate the onset of photostimulation. The histograms to the far right of each panel show matched (black) and shifted (red) correlograms computed from data collected upon stimulation in each layer. The corresponding correlation probabilities (CPs) computed from these analyses are also indicated.

the network[10–13]. Neighbouring neurons with extensively overlapping dendrites might share common input by chance, but information would be averaged across neurons to create a reliable but relatively uniform output. In the alternative scenario, there might be a fine-scale organization of connections between excitatory neurons within functional columns. The probability that two neurons are connected might be dependent on whether they share common input from other sources. This would reflect rules of connectivity that are not random but instead create substructure within each functional column. Fine-scale selectivity embedded within the columnar functional architecture might give rise to relatively independent neuronal networks that process information uniquely from their immediate neighbours.

To address these issues we took advantage of the ability of focal uncaging of glutamate ('photostimulation') to generate action potentials asynchronously in a small, spatially restricted population of neurons in rat visual cortex brain slices (see Supplementary Figs S1 and S2). By combining this type of stimulation with intracellular recordings of excitatory and inhibitory synaptic currents in pairs of adjacent layer 2/3 pyramidal neurons, we were able to use the timing of evoked synaptic currents to infer whether individual stimulated neurons provided common input to both recorded cells or if instead the recorded cells received input from separate neuronal populations. If a single presynaptic neuron is stimulated and it provides input to both recorded cells, it will generate synchronous synaptic currents; inputs from different presynaptic neurons that fire action potentials asynchronously will generate asynchronous synaptic currents.

We used established cross-correlation analysis methods[14] to normalize for synchrony resulting from time-locking of action potential generation to the stimulus (see Methods). To obtain correlation probabilities, the numbers of synchronous synaptic currents attributable to shared input were expressed as a proportion of the total numbers of evoked synaptic currents from each cell (see Methods for details). The correlation probability closely estimates the probability that when a photostimulated presynaptic neuron fires an action potential and evokes a synaptic current in one of the two recorded layer 2/3 pyramidal neurons, the same presynaptic neuron will also evoke a synaptic current in the second recorded neuron. To determine the extent of shared input from the different laminar sources to each pair of recorded layer 2/3 pyramidal cells, separate calculations of correlation probability were made based on stimulation sites in each cortical layer. For example, for the pair of layer 2/3 pyramidal neurons illustrated in Fig. 1a, the correlation probability for stimulation sites in layer 4 was 0.22, meaning that for 22% of the cases in which a layer 4 neuron was stimulated and evoked an excitatory postsynaptic current (EPSC) in one layer 2/3 cell, that same layer 4 neuron also evoked a synchronous EPSC that was detected in the other recorded layer 2/3 cell. Similarly, the correlation probability of 0.30 obtained for this same pyramidal neuron pair for stimulation sites in layer 2/3 shows that these cells share about 30% of their excitatory layer 2/3 inputs.

To test whether connected pyramidal neurons belong to functional subnetworks, we compared correlation probabilities between connected and unconnected layer 2/3 pyramidal neuron pairs. We found that the correlation probabilities for excitatory connections from layer 4 and from layer 2/3 to layer 2/3 pyramidal neuron pairs depended on whether the recorded pyramidal neurons were connected to each other. When the recorded layer 2/3 pyramids were not connected, the correlation probabilities for EPSCs were very low (Figs 1b and 2a). For unconnected cell pairs, correlation probabilities averaged 3.8 ± 1.1% (mean ± s.e.m.) for layer 2/3 stimulation sites (range −5.3 to 10.3, 17 cell pairs) and 3.6 ± 0.9% for layer 4 stimulation sites (range −2.2 to 9.1, 17 cell pairs). In sharp contrast to the low correlation probability values for cell pairs that were not connected, correlation probabilities were high when layer 2/3 pyramids were connected (Figs 1a and 2a). For connected cell pairs, correlation probabilities averaged 20.1 ± 2.7% for layer 2/3 stimulation sites (range 4.5 to 37.6, 16 cell pairs) and 16.8 ± 2.1% for layer 4 stimulation sites (range 2.9 to 30.0, 16 cell pairs). The differences in correlation probabilities for connected versus unconnected cell pairs were highly significant ($P < 0.0001$ for both layer 2/3 and layer 4 stimulation; Mann-Whitney U-test).

These data indicate that excitatory connections from layer 4 are highly selective at a fine scale, connecting preferentially to layer 2/3 pyramidal neurons that are in turn connected to each other. Furthermore, the fine-scale groupings of neurons that are defined by the selectivity of input from layer 4 are further reinforced by the fine-scale selectivity of excitatory connections within layer 2/3.

In contrast to excitatory connections from layer 4 and within layer 2/3, the specificity of excitatory connections from layer 5 was not dependent on whether the simultaneously recorded layer 2/3 pyramids were connected to each other. For stimulation sites in layer 5, correlation probabilities based on EPSCs averaged 9.8 ± 1.7% for unconnected cell pairs and 10.7 ± 1.7% for connected cell pairs (no significant difference, $P > 0.78$; Figs 1 and 2a). The finding that correlation probabilities do not differ between connected and unconnected cell pairs indicates that these connections link neurons across the fine-scale subnetworks established by the specificities of layer 4 and layer 2/3 connections.

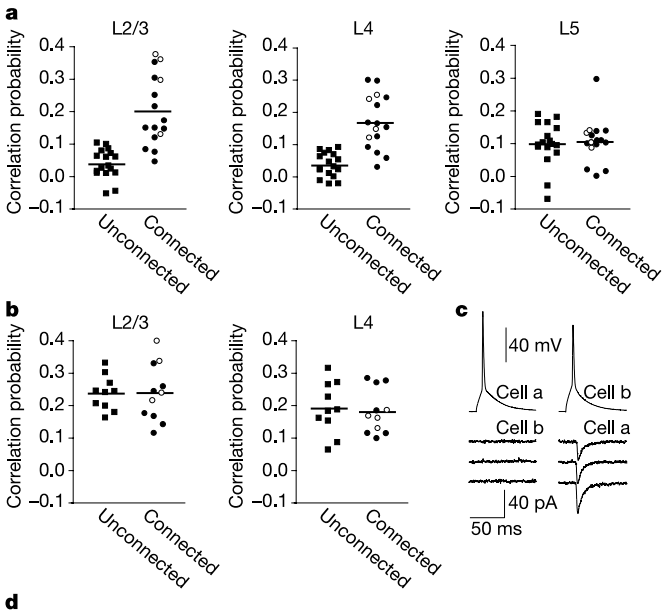

d

Properties of unitary EPSCs by dual whole-cell recordings

Tested pathway	Connection probability	Failure probability	Mean amplitude (pA)
L2/3 to L2/3	22/112 (0.2)	0.08±0.03	25.3±7.0
L4 to L2/3	10/50 (0.2)	0.04±0.01	17.1±3.1

Figure 2 Correlation probabilities for EPSCs and IPSCs in layer 2/3 pyramidal cell pairs. **a**, **b**, Correlation probabilities for EPSCs (**a**) and IPSCs (**b**) are shown separately for photostimulation sites in each cortical layer and for connected (circles) versus unconnected (squares) pairs of cells. Open circles correspond to pyramidal cells that were reciprocally connected and filled circles indicate one-way connections. Mean values for each group are indicated by horizontal lines. **c**, **d**, An experiment testing connections between pyramidal cell pairs (**c**) and summary of results (**d**). Action potentials were triggered by injecting positive current into one current-clamped cell (upper traces) while recording EPSCs in the other voltage-clamped cell (lower traces, 3 examples shown for each). The cell pair illustrated in **c** had a one-way connection from 'cell b' to 'cell a'. Connections, when present, were highly reliable for both layer 4 to layer 2/3 (4% failure) and layer 2/3 to layer 2/3 (8% failure) pairs. Connections were found in 20% of cell pairs for both layer 4 to layer 2/3 and layer 2/3 to layer 2/3 pairs.

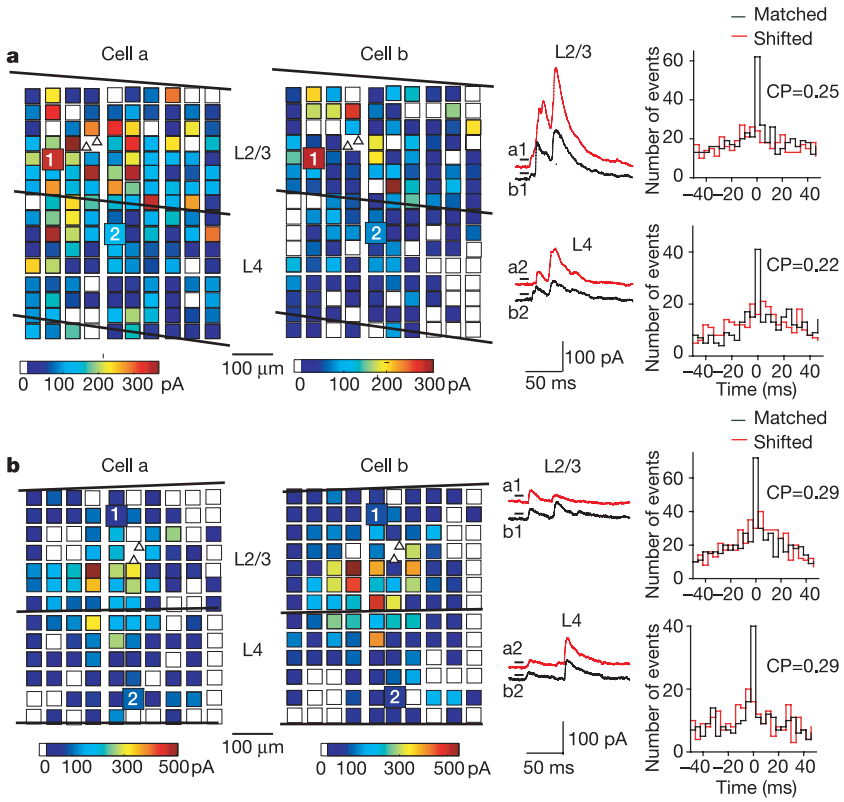

Figure 3 Cross-correlation analyses of photostimulation-evoked inhibitory postsynaptic currents (IPSCs) simultaneously recorded in adjacent pairs of layer 2/3 pyramidal neurons. See Fig. 1 legend for details.

The organization of inhibitory connections to adjacent layer 2/3 pyramidal cells was also independent from whether the layer 2/3 cells were connected. Therefore, inhibitory connections also do not respect the fine-scale groupings defined by the specificities of layer 4 and layer 2/3 excitatory connections. To estimate the extent of common inhibitory input onto adjacent pyramidal neurons from interneurons in each layer, the same photostimulation methods were employed except that the layer 2/3 pyramidal cells were voltage-clamped at 0 mV (see Methods) to allow recordings of inhibitory postsynaptic currents (IPSCs) as outward currents (Fig. 3). The correlation probabilities for IPSCs were typically high, regardless of whether the layer 2/3 pyramidal cells were connected and regardless of the layer that was stimulated (Figs 2b and 3). For connected cell pairs, correlation probabilities averaged 23.8 ± 2.7% (range 11.5 to 40.0) for stimulation sites in layer 2/3 and 18.0 ± 6.8% (range 9.8 to 28.4) for layer 4. For unconnected cell pairs the correlation probabilities averaged 23.8 ± 1.7% (range 16.2 to 33.1) for layer 2/3, and 19.1 ± 2.5% (range 6.3 to 31.6) for layer 4. There were no significant differences between connected cell pairs or between layers. Layer 5 is not included in this analysis because, as expected from previous studies[15], photostimulation in layer 5 resulted in only modest or no significant increase in IPSCs above spontaneous IPSC levels (see Methods).

It is important to note that cortical inhibition comes from diverse cell types that make synapses to different parts of the dendritic arbours of pyramidal cells and for which connections might differ in their reliability and/or detectability[16]. It is therefore possible that the IPSCs we detect during photostimulation might preferentially represent inputs from certain inhibitory cell types. For example, IPSCs detected during photostimulation could be biased towards those from basket cells (which make strong synapses close to or at the cell body)[16], relative to those from inhibitory cell types that make synapses at electrotonically distant sites[16]. Therefore, our results might not generalize to all sources of inhibition of layer 2/3 pyramidal neurons.

In summary, the results presented here indicate that excitatory connections from layer 4 to layer 2/3 pyramidal cells and within layer 2/3 are highly specific on a fine scale, creating groups of selectively interconnected neurons (Fig. 4). Such groupings

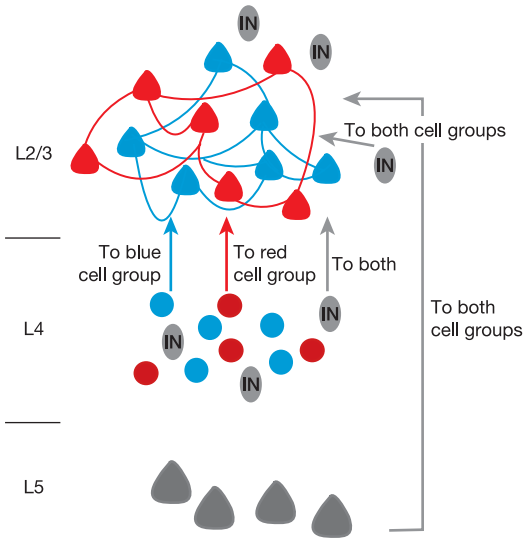

Figure 4 Schematic diagram illustrating the organization of cortical connections proposed in this study. Excitatory connections from layer 4 to layer 2/3 and within layer 2/3 define groups of selectively interconnected neurons (red or blue). The organization of excitation from layer 5 (grey triangles) and inhibition from layers 2/3 and 4 interneurons (IN, grey ovals) does not respect the fine-scale interconnected cell groups defined by excitatory connections from layer 4 and within layer 2/3.

are predicted from hebbian learning rules[17], which are likely to regulate the development and maintenance of excitatory cortical connections[18–20].

Neither inhibitory connections nor excitatory connections from layer 5 provide shared input preferentially to connected layer 2/3 pyramidal cells (Fig. 4). Instead, these connections can serve to link neurons across the fine-scale subnetworks defined by excitatory connections from layers 2–4, and might act to modulate activity between the subnetworks. These observations do not, however, rule out the possibility that these connections might be specific for modes of organization not examined in these studies. For example there could be specificity related to an organization orthogonal to the fine-scale excitatory networks in layers 2–4, or on a different spatial scale.

Previous studies, using either photostimulation or more conventional methods, have demonstrated selectivity of connections to cortical neurons of distinctly different types[15,21–28]. Here we have extended the photostimulation method to explicitly test for the possibility of fine-scale selectivity of cortical connections to neurons of the same type. We observe that the specificity of excitatory connections from layer 4 and within layer 2/3 depends on whether adjacent layer 2/3 pyramidal neurons are interconnected, independent of their locations (Fig. 4). These results therefore demonstrate selectivity of connections at a finer scale than cortical columnar architecture.

Like other species, the rat visual cortex has a columnar, retinotopic organization. But orientation-selective neurons in rat visual cortex are not organized into orientation columns; instead, adjacent neurons can be selective for disparate orientations[29]. We therefore suggest that the fine-scale specificity of excitatory connections in rat visual cortex may be related to the emergence of orientation selectivity, similar to the columnar specificity found in cats and tree shrews[3–6]. However, even in cat visual cortex where orientation columns are present, the excitatory connections from layer 4 to layer 3 are sparse; paired recordings show that layer 4 excitatory neurons connect to layer 3 pyramidal cells only 10% of the time[9]. And despite the presence of orientation columns, neighbouring neurons in cat visual cortex can differ in their selectivities for other features and sometimes demonstrate functional 'micro-organization'[30]. We therefore suggest that fine-scale selectivity of excitatory connections, embedded within the coarser columnar organization, is a common feature of cortical circuits. □

Methods

Slice preparation, photostimulation and recordings

The methods used for these experiments are similar to those reported previously[15], with some differences as detailed here. A vibratome was used to cut 300 μm thick coronal brain slices from the primary visual cortex of P21–26 Long-Evans rats. Slices were cut in artificial cerebral spinal fluid (ACSF; 124 mM NaCl, 5 mM KCl, 1.25 mM KH_2PO_4, 1.3 mM $MgSO_4$, 3.2 mM $CaCl_2$, 26 mM $NaHCO_3$ and 10 mM glucose) and stored in an interface chamber at ~34 °C for at least one hour until they were transferred to a recording chamber containing ACSF with 60–80 μM 'caged' glutamate (γ-(α-carboxy-2-nitrobenzyl) ester, trifluoroacetate, L-glutamic acid) at room temperature; this is only half the concentration of caged glutamate used in previous studies[15], and was used in order to reduce the numbers of neurons that fire action potentials synchronously (see Supplementary Fig. S2) and to reduce the size of direct responses so that postsynaptic currents (PSCs) can be detected upon stimulation at sites close to the recorded neurons. An infrared Olympus DIC microscope with a ×40, 0.8 NA water immersion lens was used to visualize and target recording electrodes to pairs of layer 2/3 pyramidal neurons with somata separated by less than 50 μm for whole-cell recordings. The mean ± SEM distances between recorded cells were 34.6 ± 3.9 μm for non-connected pairs and 35.1 ± 4.1 μm for connected pairs of neurons. Cell bodies of recorded neurons were at least 50 μm from the surface of the slice. Glass recording electrodes (4–6 MΩ resistance) were filled with an intracellular solution consisting of 130 mM K-gluconate, 6 mM KCl, 2 mM $MgCl_2$, 0.2 mM EGTA, 10 mM HEPES, 2.5 mM Na_2ATP, 0.5 mM Na_2GTP, 10 mM K-phosphocreatine and 0.3% biocytin, adjusted with KOH to pH 7.25. For some experiments in which IPSCs were recorded, potassium was replaced with cesium. All intracellular recordings had access resistances less than 20 MΩ. In all paired recordings, connections between neuron pairs were assessed by injecting current to evoke action potentials in one of the cells recorded in current-clamp while testing for PSCs during voltage-clamp recording in the other cell. For each pair, connections were tested in both directions for at least 50 trials, generating single action potentials in each presynaptic neuron. When connections were not detected with this procedure, they were also tested by stimulation in trains of 4–5 action potentials at 50 Hz to induce possible potentiation of weak connections. Control experiments measuring spatial and temporal properties of photostimulation-evoked action potentials (see Supplementary Information) used extracellular loose-patch recordings made with the same recording electrodes, except that they were filled with ACSF.

Photostimulation was achieved by uncaging glutamate with 10 ms flashes of ultraviolet light from an argon-ion laser focused through the ×40 microscope objective. This results in the generation of action potentials only in neurons with cell bodies within 100 μm (and usually less than 50 μm) of the site of uncaging (see Supplementary Fig. S1). Photostimulation-evoked synaptic currents were measured from voltage-clamped neurons, with the holding potentials at −65 mV to measure EPSCs and at 0 mV to measure IPSCs. Spontaneous synaptic currents were also recorded in interleaved trials with no stimulation.

Data analysis

Maps of photostimulation sites were aligned to laminar borders in fixed and stained tissue[15] (for example, Figs 1 and 3) and each site was assigned a laminar identity. Sites within 50 μm of laminar borders were discarded from further analyses in order to limit the number of evoked synaptic currents arising from neurons with cell bodies potentially outside the stimulated layer. The electrical recordings from photostimulation and no-stimulation (control) trials were analysed using peak analysis software from Synaptosoft and other custom software. The times of onset and amplitudes of all EPSCs or IPSCs occurring within 150 ms of stimulation were marked. Rise times of PSCs were measured as the time taken for the amplitude to increase from 10% to 90% of its peak value. Results from analyses of the laminar sources and strengths of excitatory and inhibitory input to layer 2/3 pyramidal neurons (not shown) were indistinguishable from those described previously[15], and there were no systematic differences that correlated with results from cross-correlation analyses.

Cross-correlograms of EPSCs and/or IPSCs were computed for each pair of simultaneously recorded layer 2/3 pyramidal neurons; separate correlograms were computed for stimulation sites from each cortical layer (layers 2/3, 4 and 5 for EPSCs and layers 2/3 and 4 for IPSCs). Other layers provided weak or variable input to recorded neurons, preventing evoked PSCs from being clearly distinguished from spontaneous PSCs. Correlograms were also computed for spontaneous PSCs. Cross-correlation data were binned into histograms using 4 ms bins; the central bin included values of 0 ± 2 ms. Data from the stimulation trials (from the same layer) were also used to create shifted correlograms for each layer and cell pair[14]. To calculate the correlation probability, the shifted correlogram was subtracted from the unshifted correlogram for the corresponding layer, and then the value in the central bin was divided by the average estimated total number of evoked PSCs (for the two cells) observed for all trials in the relevant layer. The average number of evoked PSCs was calculated as the total number of measured PSCs for 'cell a' minus the expected number of spontaneous PSCs for that cell, plus the same value calculated for 'cell b', divided by 2.

Received 9 September; accepted 6 December 2004; doi:10.1038/nature03252.

1. Mountcastle, V. B. Introduction. Computation in cortical columns. *Cereb. Cortex* **13,** 2–4 (2003).
2. Hubel, D. H. & Wiesel, T. N. Receptive fields, binocular interaction and functional architecture in the cat's visual cortex. *J. Physiol. (Lond.)* **160,** 106–154 (1962).
3. Chapman, B., Zahs, K. R. & Stryker, M. P. Relation of cortical cell orientation selectivity to alignment of receptive fields of the geniculocortical afferents that arborize within a single orientation column in ferret visual cortex. *J. Neurosci.* **11,** 1347–1358 (1991).
4. Ferster, D., Chung, S. & Wheat, H. Orientation selectivity of thalamic input to simple cells of cat visual cortex. *Nature* **380,** 249–252 (1996).
5. Alonso, J. M., Usrey, W. M. & Reid, R. C. Rules of connectivity between geniculate cells and simple cells in cat primary visual cortex. *J. Neurosci.* **21,** 4002–4015 (2001).
6. Mooser, F., Bosking, W. H. & Fitzpatrick, D. A morphological basis for orientation tuning in primary visual cortex. *Nature Neurosci.* **7,** 872–879 (2004).
7. Callaway, E. M. Local circuits in primary visual cortex of the macaque monkey. *Annu. Rev. Neurosci.* **21,** 47–74 (1998).
8. Thomson, A. M. & Morris, O. T. Selectivity in the inter-laminar connections made by neocortical neurones. *J. Neurocytol.* **31,** 239–246 (2002).
9. Thomson, A. M., West, D. C., Wang, Y. & Bannister, A. P. Synaptic connections and small circuits involving excitatory and inhibitory neurons in layers 2–5 of adult rat and cat neocortex: triple intracellular recordings and biocytin labelling *in vitro*. *Cereb. Cortex* **12,** 936–953 (2002).
10. Hellwig, B. A quantitative analysis of the local connectivity between pyramidal neurons in layers 2/3 of the rat visual cortex. *Biol. Cybern.* **82,** 111–121 (2000).
11. Hellwig, B., Schuz, A. & Aertsen, A. Synapses on axon collaterals of pyramidal cells are spaced at random intervals: a Golgi study in the mouse cerebral cortex. *Biol. Cybern.* **71,** 1–12 (1994).
12. Braitenberg, V. & Schuz, A. *Anatomy of the Cortex* (Springer-Verlag, Berlin, 1991).
13. Binzegger, T., Douglas, R. J. & Martin, K. A. A quantitative map of the circuit of cat primary visual cortex. *J. Neurosci.* **24,** 8441–8453 (2004).
14. Aertsen, A. M., Gerstein, G. L., Habib, M. K. & Palm, G. Dynamics of neuronal firing correlation: modulation of "effective connectivity". *J. Neurophysiol.* **61,** 900–917 (1989).
15. Dantzker, J. L. & Callaway, E. M. Laminar sources of synaptic input to cortical inhibitory interneurons and pyramidal neurons. *Nature Neurosci.* **3,** 701–707 (2000).
16. Kawaguchi, Y. & Kondo, S. Parvalbumin, somatostatin and cholecystokinin as chemical markers for specific GABAergic interneuron types in the rat frontal cortex. *J. Neurocytol.* **31,** 277–287 (2002).
17. Hebb, D. O. *The Organization of Behavior* (Wiley, New York, 1949).
18. Yoshimura, Y., Ohmura, T. & Komatsu, Y. Two forms of synaptic plasticity with distinct dependence on age, experience, and NMDA receptor subtype in rat visual cortex. *J. Neurosci.* **23,** 6557–6566 (2003).
19. Sur, M., Schummers, J. & Dragoi, V. Cortical plasticity: time for a change. *Curr. Biol.* **12,** R168–R170 (2002).

20. Katz, L. C. & Shatz, C. J. Synaptic activity and the construction of cortical circuits. *Science* **274,** 1133–1138 (1996).
21. Sawatari, A. & Callaway, E. M. Diversity and cell type specificity of local excitatory connections to neurons in layer 3B of monkey primary visual cortex. *Neuron* **25,** 459–471 (2000).
22. Schubert, D., Kotter, R., Zilles, K., Luhmann, H. J. & Staiger, J. F. Cell type-specific circuits of cortical layer IV spiny neurons. *J. Neurosci.* **23,** 2961–2970 (2003).
23. Agmon, A. & Connors, B. W. Correlation between intrinsic firing patterns and thalamocortical synaptic responses of neurons in mouse barrel cortex. *J. Neurosci.* **12,** 319–329 (1992).
24. Gibson, J. R., Beierlein, M. & Connors, B. W. Two networks of electrically coupled inhibitory neurons in neocortex. *Nature* **402,** 75–79 (1999).
25. Gonchar, Y. & Burkhalter, A. Connectivity of GABAergic calretinin-immunoreactive neurons in rat primary visual cortex. *Cereb. Cortex* **9,** 683–696 (1999).
26. Gonchar, Y. & Burkhalter, A. Distinct GABAergic targets of feedforward and feedback connections between lower and higher areas of rat visual cortex. *J. Neurosci.* **23,** 10904–10912 (2003).
27. Meskenaite, V. Calretinin-immunoreactive local circuit neurons in area 17 of the cynomolgus monkey, Macaca fascicularis. *J. Comp. Neurol.* **379,** 113–132 (1997).
28. Staiger, J. F. *et al.* Innervation of interneurons immunoreactive for VIP by intrinsically bursting pyramidal cells and fast-spiking interneurons in infragranular layers of juvenile rat neocortex. *Eur. J. Neurosci.* **16,** 11–20 (2002).
29. Girman, S. V., Sauve, Y. & Lund, R. D. Receptive field properties of single neurons in rat primary visual cortex. *J. Neurophysiol.* **82,** 301–311 (1999).
30. DeAngelis, G. C., Ghose, G. M., Ohzawa, I. & Freeman, R. D. Functional micro-organization of primary visual cortex: receptive field analysis of nearby neurons. *J. Neurosci.* **19,** 4046–4064 (1999).

Supplementary Information accompanies the paper on **www.nature.com/nature**.

Acknowledgements We are grateful for support from the National Institutes of Health. We thank Y. Komatsu and F. Briggs and members of the Callaway laboratory for discussions.

Competing interests statement The authors declare that they have no competing financial interests.

Correspondence and requests for materials should be addressed to E.M.C. (callaway@salk.edu).

Different time courses of learning-related activity in the prefrontal cortex and striatum

Anitha Pasupathy & Earl K. Miller

The Picower Center for Learning and Memory, RIKEN-MIT Neuroscience Research Center and Department of Brain and Cognitive Sciences, Massachusetts Institute of Technology, Cambridge, Massachusetts 02139 USA

To navigate our complex world, our brains have evolved a sophisticated ability to quickly learn arbitrary rules such as 'stop at red'. Studies in monkeys using a laboratory test of this capacity—conditional association learning—have revealed that frontal lobe structures (including the prefrontal cortex) as well as subcortical nuclei of the basal ganglia are involved in such learning[1–5]. Neural correlates of associative learning have been observed in both brain regions[6–14], but whether or not these regions have unique functions is unclear, as they have typically been studied separately using different tasks. Here we show that during associative learning in monkeys, neural activity in these areas changes at different rates: the striatum (an input structure of the basal ganglia) showed rapid, almost bistable, changes compared with a slower trend in the prefrontal cortex that was more in accordance with slow improvements in behavioural performance. Also, pre-saccadic activity began progressively earlier in the striatum but not in the prefrontal cortex as learning took place. These results support the hypothesis that rewarded associations are first identified by the basal ganglia, the output of which 'trains' slower learning mechanisms in the frontal cortex[15].

The prefrontal cortex (PFC) is a cortical area important for the organization of goal-directed, rule-based behaviours; the basal ganglia are a group of subcortical nuclei long associated with the control of volitional movements[1–3,16–18]. Both of these areas receive inputs from many brain systems (for example, sensory, motor and reward), which makes them well suited for roles in learning. Their anatomy also suggests a close relationship—the PFC and basal ganglia are interconnected in cortico-basal ganglionic 'loops'[19,20]—but the nature of this interaction is still unclear. Some results have led to the suggestion of a sequential relationship, in which the PFC is involved in new learning and the basal ganglia are subsequently involved in consolidating familiar routines into automatic habits[21,22]. Another hypothesis, not necessarily incompatible with the one above, suggests a dominant role for the basal ganglia in new learning[15,23] due to its anatomical architecture and the membrane properties of striatal spiny neurons. These hypotheses lead to specific predictions about the time course of learning in these areas: based on the first hypothesis, the PFC is predicted to lead the basal ganglia; based on the second hypothesis, the basal ganglia lead the PFC. Here, we report evidence in favour of the latter event; that is, learning-related changes appear sooner and progress more rapidly in the striatum than the PFC.

To test these hypotheses, we simultaneously recorded neural activity from the dorsolateral PFC (areas 9 and 46) and the head and body of the caudate nucleus, a part of the striatum that receives direct projections from, and indirectly projects to, the PFC[19,20] (see Methods). Monkeys learned associations between each of two visual cues and two saccadic eye movements (right and left, Fig. 1a). Monkeys were familiar with the task, but each day two novel cues were used and their associations learned by trial and error using juice reward as feedback. Once the cue–saccade associations had been learned, they were reversed without warning and the opposite pairing was then learned (see Supplementary Note 1).

Figure 1b (left) shows the average behavioural performance before and after the reversals. Saccade choices dropped to about 0% correct for the first few trials after the reversal because the previous associations were still being followed. Then, performance jumped to chance (50%) followed by a slow increase with trial number. Likewise, reaction time increased by an average of about

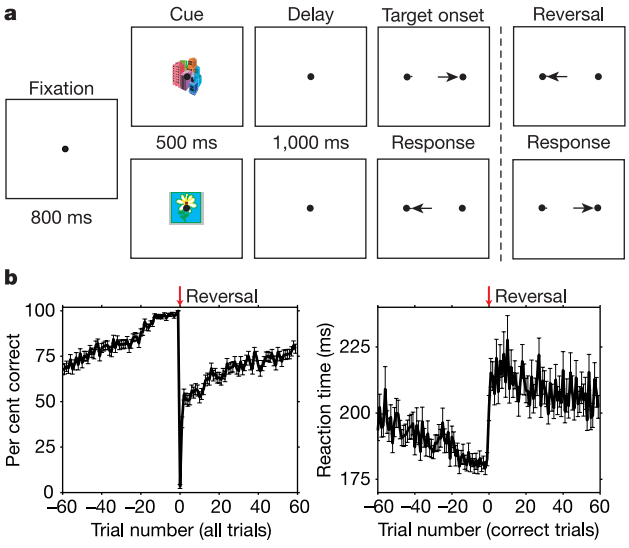

Figure 1 Task and behaviour. **a**, One of two initially novel cues was briefly presented at centre of gaze followed by a memory delay and then presentation of two target spots on the right and left. Saccade to the target associated with the cue at that time was rewarded. After this was learned, the cue–saccade associations were reversed and re-learned. **b**, Average per cent correct performance (left) and reaction time (right) across sessions and blocks as a function of trial number (left: all trials; right: correct trials only) during learning for two monkeys. Zero (indicated by red arrow) represents first trial after reversal. Error bars show standard error of the mean.